Kaposi's Sarcoma–Associated Herpesvirus Viral IFN Regulatory Factor 3 Stabilizes Hypoxia-Inducible Factor-1α to Induce Vascular Endothelial Growth Factor Expression

Young C. Shin,[1] Chul-Hyun Joo,[2] Michaela U. Gack,[1] Hye-Ra Lee,[1] and Jae U. Jung[1]

[1]Department of Microbiology and Molecular Genetics and Tumor Virology Division, New England Primate Research Center, Harvard Medical School, Southborough, Massachusetts and [2]Department of Microbiology, University of Ulsan College of Medicine, Seoul, Korea

Abstract

Kaposi's sarcoma–associated herpesvirus (KSHV) is the etiologic agent associated with Kaposi's sarcoma, primary effusion lymphoma, and multicentric Castleman's disease. Hypoxia-inducible factor-1 (HIF-1) is the master regulator of both developmental and pathologic angiogenesis, composed of an oxygen-sensitive α-subunit and a constitutively expressed β-subunit. HIF-1 activity in tumors depends on the availability of the HIF-1α subunit, the levels of which are increased under hypoxic conditions. Recent studies have shown that HIF-1 plays an important role in KSHV reactivation from latency and pathogenesis. Here, we report a novel mechanism by which KSHV activates HIF-1 activity. Specific interaction between KSHV viral IFN regulatory factor 3 (vIRF3) and the HIF-1α subunit led to the HIF-1α stabilization and transcriptional activation, which induced vascular endothelial growth factor expression and ultimately facilitated endothelial tube formation. Remarkably, the central domain of vIRF3, containing double α-helix motifs, was sufficient not only for binding to HIF-1α but also for blocking its degradation in normoxic conditions. This indicates that KSHV has developed a unique mechanism to enhance HIF-1α protein stability and transcriptional activity by incorporating a viral homologue of cellular *IRF* gene into its genome, which may contribute to viral pathogenesis. [Cancer Res 2008;68(6):1751–9]

Introduction

Kaposi's sarcoma–associated herpesvirus (KSHV), or human herpesvirus-8, is the etiologic agent of Kaposi's sarcoma (1), primary effusion lymphoma (PEL; ref. 2), and multicentric Castleman's disease (MCD; ref. 3). Various cytokines (viral and cellular) and viral oncogenes provide a favorable environment for the growth of these tumors. Kaposi's sarcoma is a hypervascular endothelial tumor (4) frequently found in acquired immunodeficiency syndrome–associated neoplasm (5), and it is composed of mixed cell types, including fibroblasts, smooth muscle cells, inflammatory cells, and endothelial cells (6). Particularly, spindle cells of endothelial origin are the most common cell type in Kaposi's sarcoma (7) and produce a variety of proinflammatory and angiogenic factors, which are likely the driving forces of Kaposi's sarcoma lesion (8). Among these, vascular endothelial growth factor (VEGF) secreted by the proliferating spindle cells has been attributed to the abundant vasculature of Kaposi's sarcoma (4).

In accordance with the hypervascular nature of Kaposi's sarcoma, it has been shown that many KSHV-encoded proteins function to stimulate angiogenesis. For example, KSHV viral G protein–coupled receptor (vGPCR) encoded by open reading frame (ORF) 74 is a constitutively active homologue of the human interleukin (IL)-8 receptor (9). vGPCR activates c-Jun NH_2-terminal kinase/stress-activated protein kinase and p38 mitogen-activated protein kinase kinases in an agonist-independent way and up-regulates the transcription of VEGF (10, 11). Moreover, the expression of vGPCR in transgenic mice leads to oncogenic transformation that closely resembles Kaposi's sarcoma lesions (12), inducing strong angiogenesis and spindle cell proliferation (12, 13). It also has been shown that the K1 and viral IL-6 proteins of KSHV induce VEGF production (14, 15). Because VEGF is a potent angiogenic stimulator and Kaposi's sarcoma spindle cell growth factor (16), it is not surprising to find VEGF induction by these KSHV-encoded proteins, although the detailed mechanism by which they accomplish this may differ from one to another.

VEGF is highly induced in hypoxic conditions where cell encounters a limited oxygen concentration and plays a critical role in tumor growth and maintenance. Hypoxia-inducible factor 1 (HIF-1), composed of α- and β-subunit (17), is the key regulator of cellular responses to low oxygen concentration. Under normal oxygen concentrations, HIF-1α undergoes rapid ubiquitination by the von Hippel-Lindau (VHL) complex followed by proteasomal degradation (18). During this process, hydroxylation of the proline residues (Pro^{406} and Pro^{564}) located in the oxygen-dependent degradation domain (ODD) of HIF-1α is critical for the interaction of HIF-1α and VHL (19). Under hypoxic conditions, however, hydroxylation of HIF-1α is impaired, leading to prevention of VHL from targeting HIF-1α degradation (20). The accumulated HIF-1α moves into the nucleus and forms a stable heterodimer with its constitutive β-subunit, HIF-1β, to induce many of downstream target genes, including VEGF (21), erythropoietin (22), and glycolytic enzymes (23). Expression of these target genes promotes the survival of hypoxic cells by up-regulating angiogenesis and anaerobic glycolysis. In fact, the stabilization of HIF-1α protein levels is often observed in many cancer cells, especially those with a VHL deficiency. Renal cell carcinoma is one of the most well-characterized angiogenic tumors caused by elevated HIF-1α protein levels due to the genetic inactivation of VHL (24).

KSHV *viral IFN regulatory factor 3* (*vIRF3*), also known as the latency-associated nuclear antigen 2 (LANA2), has been identified as a latently expressed gene in PEL and MCD. However, vIRF3 protein has not been detected in Kaposi's sarcoma lesion by

Note: Y.C. Shin and C-H. Joo contributed equally to this work.

Requests for reprints: Young C. Shin, Tumor Virology Division, New England Primate Research Center, Harvard Medical School, 1 Pine Hill Drive, Southborough, MA 01772. Phone: 508-786-1472; Fax: 508-786-1416; E-mail: young_shin@hms.harvard.edu.

doi:10.1158/0008-5472.CAN-07-2766

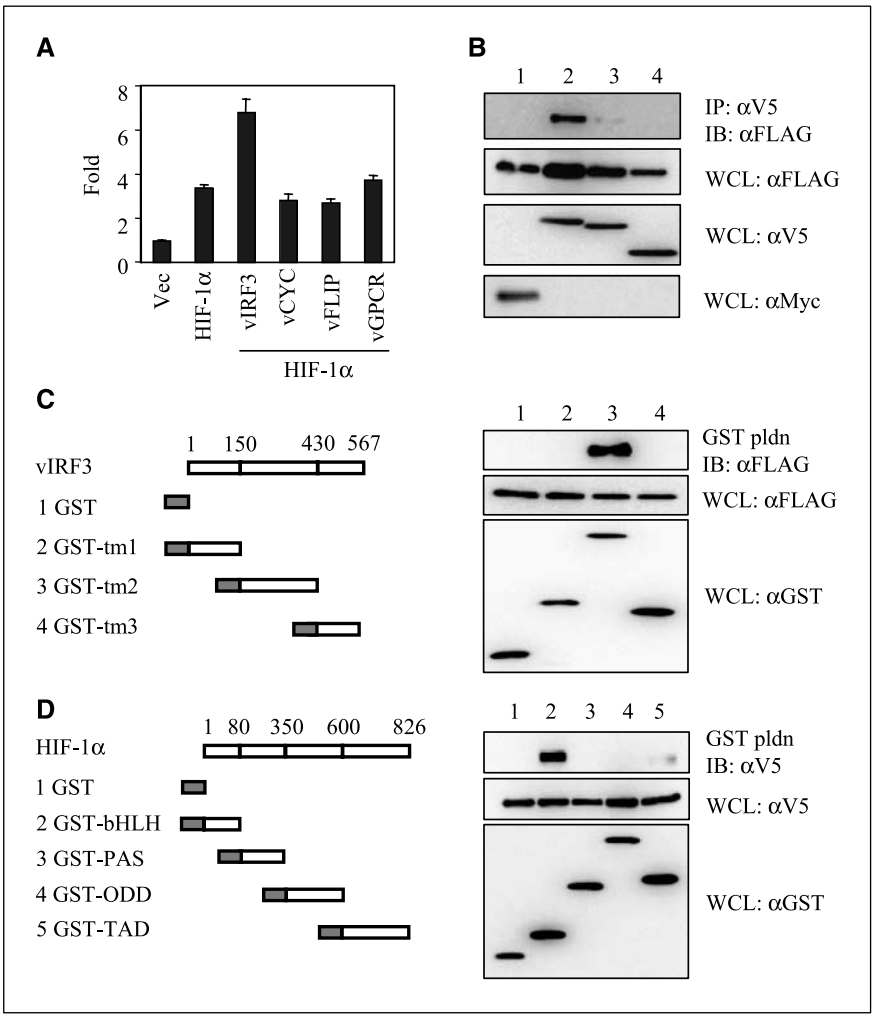

Figure 1. vIRF3 interacts with HIF-1α and activates its transcriptional activity. *A,* activation of HIF-1α transcriptional activity by vIRF3. 293T cells were transfected with FLAG-HIF-1α expression plasmid, HRE-luciferase plasmid, and pRL-SV40 plasmid along with KSHV gene expression plasmid and harvested at 48 h after transfection. Firefly luciferase values were normalized to *Renilla* luciferase values and presented as a fold induction. *B,* interaction of vIRF3 wt and mutants with HIF-1α. 293T cells were seeded onto 10-cm tissue culture dishes and transfected with FLAG-HIF-1α (18 μg) together with V5-vIRF3 wt or mutants (9 μg). For the immunoprecipitation (*IP*) control, Myc-vIRF3 wt (9 μg) was expressed together with FLAG-HIF-1α. At 48 h after transfection, cell lysates were used for immunoprecipitation with anti-V5 antibody followed by immunoblotting (*IB*) with anti-FLAG antibody. Whole-cell lysates (*WCL*) were used for immunoblotting with anti-Myc, anti-V5, or anti-FLAG antibody to show expression of vIRF3 and HIF-1α. *Lane 1,* Myc-vIRF3 wt; *lane 2,* V5-vIRF3 wt; *lane 3,* V5-vIRF3 hm; *lane 4,* V5-vIRF3 dd2. *C,* the central region of vIRF3 interacts with HIF-1α. *Left,* schematic representation of vIRF3 truncation mutants (tm1, tm2, and tm3) fused with the NH_2-terminal GST mammalian protein. *Numbers,* amino acid residues of vIRF3. *Right,* interaction of vIRF3 truncation mutants with HIF-1α. 293T cell lysates were transfected with FLAG-HIF-1α along with GST-vIRF3 fusions and harvested at 48 h after transfection and subjected to GST pull-down followed by immunoblotting with anti-FLAG antibody. Whole-cell lysates were also used for immunoblotting with anti-FLAG and anti-GST antibodies to detect HIF-1α and GST-vIRF3 fusion expression. *D,* the NH_2-terminal bHLH domain and, to a lesser extent, the COOH-terminal TAD of HIF-1α interact with vIRF3. *Left,* schematic representation of HIF-1α truncation mutants. Each functional domain of HIF-1α (bHLH, PAS, ODD, or TAD) was fused with GST at its NH_2-terminal region. *Numbers,* amino acid residues in each truncation. *Right,* interaction of HIF-1α mutants with vIRF3. At 48 h after transfection with V5-vIRF3 wt along with GST-HIF-1α fusions, 293T cell lysates were used for GST pull-down followed by immunoblotting with anti-V5 antibody. Whole-cell lysates were also used for immunoblotting with anti-V5 and anti-GST antibody to show vIRF3 and GST-HIF-1α fusion expression. *Lane 1,* GST; *lane 2,* GST-bHLH; *lane 3,* GST-PAS; *lane 4,* GST-ODD; *lane 5,* GST-TAD.

immunohistochemistry (25). vIRF3 exhibits sequence homology with cellular IRF, especially its COOH terminus with that of cellular IRF4 (26). However, five tryptophan residues in the DNA-binding domain of cellular IRFs are not conserved in vIRF3. It has been shown that vIRF3 binds and inhibits p53 transcription factor (25). vIRF3 also inhibits PKR-mediated apoptosis (27) and deregulates IFN-α promoter activity by interacting with cellular IRF3, IRF7, and cyclic AMP-responsive element binding protein–binding protein/p300 (28, 29).

In this report, we showed that the KSHV vIRF3 protein targeted cellular HIF-1α, which led to an increase of HIF-1α protein stability and its transcriptional activity. Consequently, vIRF3 expression resulted in the up-regulation of VEGF and facilitated endothelial tube formation. Collectively, this indicates that KSHV vIRF3 not only deregulates IFN/p53-mediated innate immune control but also enhances HIF-1α–mediated cell proliferation, suggesting the important role of vIRF3 in the KSHV life cycle.

Materials and Methods

Plasmids, cell culture, and transfection. The plasmid encoding vIRF3 was kindly provided by Dr. Patrick S. Moore (University of Pittsburgh, Pittsburgh, PA). The plasmids encoding HIF-1α and hypoxia response element (HRE)-luciferase were provided by Dr. Chris Bradfield (University of Wisconsin, Madison, WI). HIF-1α and vIRF3 were cloned

into pEFIRES-P vector (30) with a COOH-terminal FLAG tag or a V5 tag, respectively. The vIRF3 helix mutant (hm) was constructed using a site-directed mutagenesis kit (Stratagene). In this mutant, all of the negatively charged amino acids in the helix region (amino acids 240–280; see the main text for detail) were substituted with neutral amino acids. Overall, the original amino acid sequence of VEDDLTLLDKESACALMYHVG-QEMDMLMRAMCDEDLFDLL was changed into VENNLTLLNKQSACAL-MYHVGQEMDMLMRAMCNQNLFNLL (the mutated residues were underlined). The helix deletion mutant of vIRF3 (dd2) was constructed by ligating PCR-amplified vIRF3 fragments spanning amino acids 1 to 219 and 291 to 567, respectively. The glutathione *S*-transferase (GST)–tagged truncation mutants of vIRF3 and HIF-1α were constructed by the PCR amplification of each corresponding fragment followed by cloning into pEBG vector. The specific sites of truncation were schematically represented (Fig. 1*C* and *D*). The plasmid DNA encoding each protein was purified by standard cesium chloride gradient ultracentrifugation.

SLK human endothelial cells and 293T cells were maintained in DMEM supplemented with 10% fetal bovine serum, 2 mmol/L glutamine, and penicillin (100 units/mL)/streptomycin (100 μg/mL).

Construction of stable cell lines. The DNA encoding vIRF3 wild-type (wt) and its mutants was cloned into the pBabe-puro vector. Each plasmid was transfected into AmphoPack-293 cells (Clontech) to produce the retroviruses. For the control, an empty pBabe-puro vector was transfected. The SLK cells were infected with retroviruses encoding each construct and selected with 2.0 μg/mL puromycin (Sigma). For the construction of TRExBCBL1 stable cells, *vIRF3* gene was cloned into pcDNA5/FRT/TO vector (Invitrogen) and electroporated into TRExBCBL1 cells followed by antibiotic selection using 200 μg/mL hygromycin (Invitrogen).

Reagents and chemicals. Cells were treated with 50 μmol/L MG 132 (Calbiochem), 50 μg/mL cycloheximide (Sigma), and 100 μmol/L cobalt chloride (Sigma) for the indicated times. The antibodies used in this study were GST (G1160; Sigma), β-actin (AC-15; Abcam), HIF-1α (BD Transduction Laboratories), vIRF3 (CM-A807; Novus Biologicals), and VEGF (MAB 293; R&D Systems).

Luciferase reporter assay. 293T cells were seeded onto 24-well plates (10^5 per well) and then transfected 20 hours later with 500 ng of pEFIRES-HIF-1α, 10 ng of pGL3-HRE-luciferase reporter plasmid, 50 ng of *Renilla* luciferase plasmid (pRL-SV40; Promega), and 32 ng of plasmid encoding each KSHV gene. The total amount of DNA in each transfection was adjusted to the same by adding empty pEFIRES-P vector. At 48 hours after transfection, cells were lysed with passive lysis buffer (Promega). Firefly and *Renilla* luciferase activity was measured with a luminometer using a dual-luciferase assay kit (Promega). Firefly luciferase activity was normalized to *Renilla* luciferase activity for the transfection efficiency. Each experiment was performed in triplicate and the relative average fold with respect to control cells was represented with SD.

Real-time reverse transcription-PCR. The mRNA of SLK stable cells was purified using the RNeasy Plus Miniprep kit (Qiagen) and quantified using UV spectrophotometry. The first strand was synthesized from 5 μg of purified mRNA using SuperScript III reverse transcriptase (Invitrogen) and gene-specific reverse primers (see below). Real-time PCR was executed on a MyiQ system (Bio-Rad) using MyiQ SYBR Green II Master Mix (Bio-Rad). The efficiencies of each primer set were calculated from the serial dilution curves and the relative amounts of mRNA were calculated by using Pfaffle's method as described (31). The primers used for the real-time PCR were as follows: HIF-1α, GATTTAGCATGTAGACTGCTG (forward) and TCAGT-TAACTTGATCCAAAGC (reverse); β-actin, TGGACATCCGCAAAGACCTG (forward) and CCGATCCACACGGAGTACTT (reverse).

Confocal microscopy. The SLK cells (1×10^5) stably expressing empty vector, vIRF3 wt, or its mutants were seeded onto each well of Lab-Tek II four-well chamber slides (Nalge Nunc International). The following day, they were fixed with 4% paraformaldehyde for 20 minutes and permeabilized with 0.2% Triton X-100 in PBS for 20 minutes. To detect HIF-1α protein, HIF-1α antibody (BD Transduction Laboratories) was diluted (1:200) with PBS containing 3% bovine serum albumin (BSA) and incubated at room temperature for 60 minutes followed by washing with PBS. Alexa Fluor 488–conjugated anti-mouse secondary antibody (Invitrogen) was diluted (1:1,000) with PBS and incubated at room temperature for 30 minutes followed by extensive washing with PBS containing 0.2% Triton X-100. For the detection of the vIRF3 protein, monoclonal anti-vIRF3 antibody (Novus Biologicals) was diluted (1:1,000) with PBS containing 3% BSA and incubated at room temperature for 30 minutes followed by washing with PBS. Alexa Fluor 568–conjugated anti-mouse secondary antibody (Invitrogen) was diluted (1:1,000) with PBS and incubated for 30 minutes. After washing thrice with PBS containing 0.2% Triton X-100, nuclei were stained with Topro-3 (1:5,000 dilution; Invitrogen) for 5 minutes followed by washing with PBS. Confocal microscopy was performed as previously described (32).

Immunoblotting, immunoprecipitation, and GST pull-down. Cells were harvested, resuspended with lysis buffer [50 mmol/L Tris (pH 8.0), 150 mmol/L NaCl, 0.5% Triton X-100] containing protease inhibitors (Sigma), and centrifuged ($12,000 \times g$) for 5 minutes. The supernatants were transferred to a new tube and their respective protein levels were measured using a bicinchoninic acid protein assay kit (Pierce) and normalized. The equal volume of 2× SDS sample buffer was added to each lysate and the samples were boiled for 5 minutes before SDS-PAGE analysis.

For immunoprecipitation and GST pull-down, cell lysates were precleared with Sepharose beads for 1 hour at 4°C. For GST pull-down, glutathione beads (Amersham) were added into the precleared cell lysates and mixed for 3 hours at 4°C. For immunoprecipitation, FLAG (Sigma) or V5 antibody (Invitrogen) was added into the precleared cell lysates and incubated for 3 hours at 4°C followed by addition of protein A/G agarose (Pierce) and mixed for an additional 2 hours. The beads were washed thrice with cold lysis buffer. The purified proteins were eluted with SDS sample buffer, separated by SDS-PAGE, and transferred to polyvinylidene difluoride membrane (Roche). The membrane was subjected to immunoblot assay. Briefly, the membranes were blocked with PBS containing 5% skim milk for 30 minutes at room temperature and incubated with the appropriate primary antibody from 1 hour to overnight followed by 1 hour of incubation with the appropriate horseradish peroxidase (HRP)-conjugated secondary antibody. Specific signals were detected by enhanced chemiluminescence system.

RNase protection assay. The total cellular RNA from SLK stable cells was extracted using Trizol reagent (Invitrogen) according to the manufacturer's instructions. The [^{32}P]UTP-labeled antisense RNA probe was synthesized by *in vitro* transcription of the hAngio-1 multiprobe template set (BD Biosciences). This probe was mixed with 15 μg of total isolated RNA and incubated for 3 minutes at 90°C and then for 16 hours with a gradual temperature reduction to 56°C. RNase protection assay (RPA) was carried out using a RPA kit (BD PharMingen) according to the manufacturer's instructions. The samples were separated on a 6% urea-Tris-borate EDTA acrylamide gel (Invitrogen). The gel was dried and exposed using a phosphoimager (BAS 2000, Fuji Photo Film Co.).

Cytokine antibody array and VEGF ELISA. The cultured supernatants taken from confluent SLK stable cells were adjusted by appropriate dilutions based on the cell number. They were then incubated for 2 hours with TranSignal human cytokine antibody array membranes (Panomics) to permit cytokine binding to the immobilized antibodies on the membrane. The captured cytokines on the membrane were incubated with a mixture of biotin-labeled anti-cytokine antibodies followed by streptavidin-HRP chemiluminescent detection. For the detection of VEGF-secreted protein, culture supernatants were processed using a VEGF Accucyte enzyme immunoassay kit (Calbiochem) and the amount of VEGF in each sample was calculated using a standard curve obtained in a parallel experiment.

Endothelial tube formation assay. Human umbilical vascular endothelial cells (HUVEC) were purchased (Cambrex) and maintained in EBM-2 medium supplemented with EGM-2 SingleQuots (Cambrex). To circumvent source-to-source variations, HUVECs were immortalized with retroviruses (BD Biosciences) encoding E6/E7 proteins of human papillomavirus and selected with 200 μg/mL G418. Tube formation assay on extracellular matrix (ECM) gel (Sigma) was performed according to the manufacturer's protocol with minor modifications. Briefly, immortalized HUVECs (3×10^4) resuspended with 150 μL of EBM-2 medium were seeded on ECM gel solidified in 96-well tissue culture plate. Conditioned medium (50 μL) from the supernatant of each SLK stable cells was added. For the control

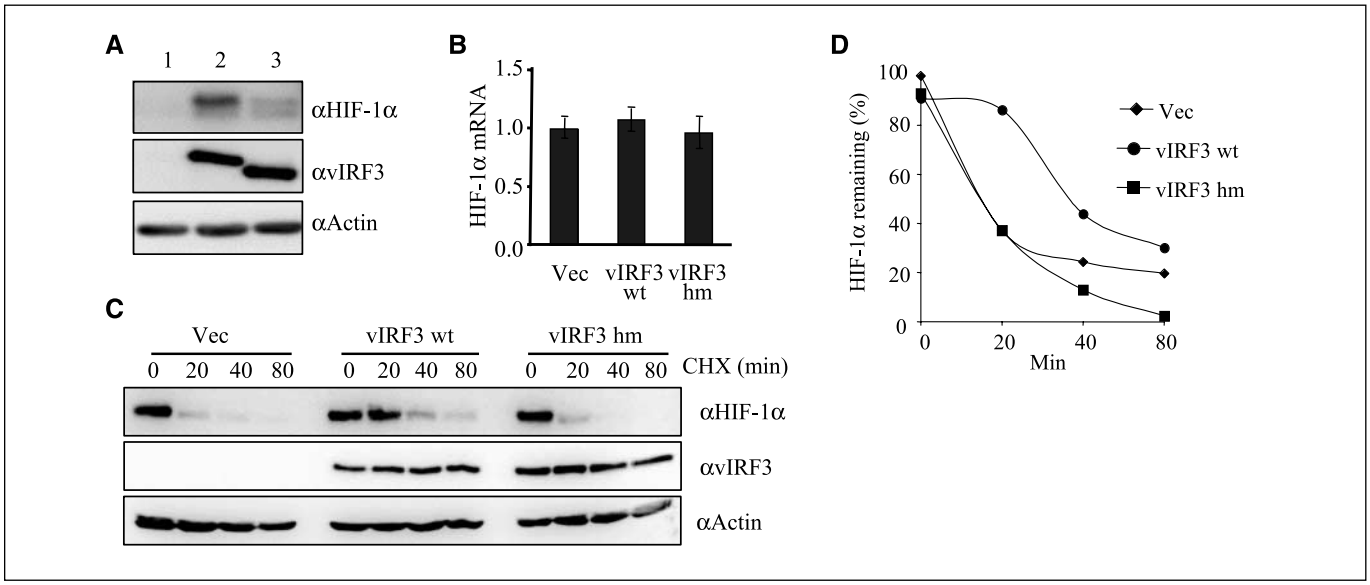

Figure 2. vIRF3 induces HIF-1α protein stability. *A,* vIRF3 enhances endogenous HIF-1α protein level. Lysates of SLK cells stably expressing empty vector (*lane 1*), vIRF3 wt (*lane 2*), and vIRF3 hm (*lane 3*) were analyzed by immunoblotting with anti-HIF-1α, anti-vIRF3, and anti-actin antibodies to detect their expression. *B,* no effect of vIRF3 on HIF-1α mRNA level. Total RNA from SLK cells stably expressing vector (*lane 1*), vIRF3 wt (*lane 2*), or vIRF3 hm (*lane 3*) was used for quantitative real-time RT-PCR with HIF-1α–specific and actin-specific primers. *C,* increase of HIF-1α protein stability in vIRF3-expressing cells. SLK cells stably expressing empty vector, vIRF3 wt, or vIRF3 hm were incubated with cobalt chloride (100 μmol/L) for 8 h before cycloheximide (*CHX*) treatment. Cells were then harvested at the indicated time points and analyzed by immunoblotting using anti-HIF-1α, anti-vIRF3, and anti-actin antibodies. *D,* quantitation of HIF-1α protein amount. The HIF-1α bands from *C* were quantified using ImageGauge program.

experiments, 50 μL of DMEM or DMEM supplemented with VEGF was added, respectively. For the neutralization of VEGF, anti-VEGF antibody was added (6 μg/well). Cells were incubated in a CO_2 incubator for 24 hours at 37°C and then examined for tube formation with a light microscope.

Results

vIRF3 interacts with HIF-1α. The expression and transcriptional activity of HIF-1α are up-regulated in KSHV-infected endothelial cells (33). To identify KSHV proteins that affect HIF-1α activity, we surveyed several KSHV proteins for their potential effects on HIF-1α activity using the luciferase construct containing six repeats of HRE. Among the several KSHV genes tested, *vIRF3* but not *vCyclin, vFLIP*, or *vGPCR* was found to activate the HRE-driven promoter activity to a detectable level (Fig. 1*A*; data not shown). To further delineate how vIRF3 activated HRE promoter activity, we tested whether vIRF3 interacts with HIF-1α to activate its transcriptional activity. Coimmunoprecipitation of 293T cells transfected with V5-vIRF3 and FLAG-HIF-1α showed the efficient vIRF3 interaction with HIF-1α (Fig. 1*B, lane 2*). To further define the region of vIRF3 required for HIF-1α interaction, GST-vIRF3 truncation mutants were used for GST pull-down assay (Fig. 1*C*). This showed that the central region (amino acids 150–430) of vIRF3, called tm2 mutant, was sufficient for the interaction with FLAG-HIF-1α (Fig. 1*C, lane 3*). We have previously shown that the double α-helix motifs (240–280 amino acids) within the central region of vIRF3 are responsible for the interaction with cellular IRF7 (29). To test whether these double α-helix motifs are also necessary for the interaction with HIF-1α, V5-vIRF3 hm and V5-vIRF3 dd2 (Δ220–290 amino acids) were used for FLAG-HIF-1α interaction. Whereas vIRF3 hm displayed a minimal binding activity to HIF-1α, vIRF3 dd2 mutant showed no interaction with HIF-1α (Fig. 1*B, lanes 3* and *4*). This indicates that, as seen with vIRF3 interaction with cellular IRF7 (29), the double α-helix motifs of vIRF3 are critical for its interaction with HIF-1α.

HIF-1α contains an NH_2-terminal basic helix-loop-helix (bHLH), a Per/Arnt/Sim (PAS) domain, an ODD, and a COOH-terminal transactivation domain (TAD; Fig. 1*D*; ref. 34). To identify the vIRF3-binding region in HIF-1α, GST-HIF-1α mammalian fusion proteins containing each domain of HIF-1α were generated and used for GST pull-down assay. The NH_2-terminal bHLH and, to a lesser extent, the COOH-terminal TAD of HIF-1α were sufficient for the interaction with vIRF3 (Fig. 1*D*). In contrast, the GST control, GST-PAS, and GST-ODD of HIF-1α were not capable of interacting with vIRF3 under similar conditions (Fig. 1*D*).

vIRF3 stabilizes HIF-1α protein. HIF-1α undergoes rapid ubiquitination by the VHL complex followed by proteasomal degradation (18). To examine whether vIRF3 interaction with HIF-1α affected HIF-1α protein level, we first generated Kaposi's sarcoma–derived SLK cell lines expressing vector, vIRF3 wt, or vIRF3 hm. Immunoblotting with HIF-1α antibody showed that vIRF3 wt expression markedly increased HIF-1α protein amount in SLK cells, whereas vIRF3 hm expression did only at a minimal level under the same conditions (Fig. 2*A*). Real-time reverse transcription-PCR (RT-PCR) analysis showed that HIF-1α mRNA levels were relatively similar in all three stable cell lines (Fig. 2*B*), suggesting that vIRF3 affects HIF-1α expression at the posttranscriptional level.

To examine whether vIRF3 affected HIF-1α protein stability, we used the cycloheximide treatment that blocks *de novo* protein synthesis. Because the HIF-1α protein was almost undetectable or extremely low in SLK-vector cells and in SLK-vIRF3 hm cells, respectively, we first treated SLK cells with cobalt chloride that blocks prolyl hydroxylase-mediated proteasomal degradation (35). Under these conditions, SLK-vIRF3 wt cells showed the marked increase of HIF-1α stability compared with SLK-vector and SLK-vIRF3 hm cells (Fig. 2*C* and *D*). We further examined endogenous HIF-1α level in KSHV-infected TRExBCBL1 cells. Although KSHV-infected BCBL1 cells carry a low level of vIRF3 expression,

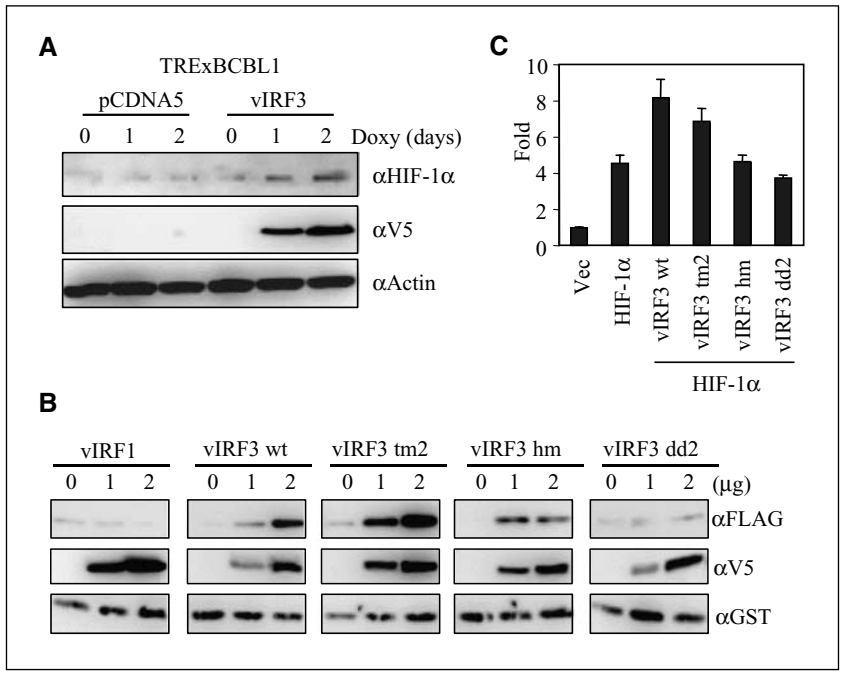

Figure 3. vIRF3 expression enhances HIF-1α protein level and transcriptional activity. *A,* vIRF3 expression increases endogenous HIF-1α protein amount in KSHV-infected BCBL1 cells. TRExBCBL1-pcDNA5 and TRExBCBL1-V5-vIRF3 cells were treated with doxycycline (*Doxy*) for the indicated times (day) and their lysates were used for immunoblotting with anti-HIF-1α, anti-V5, and anti-actin antibodies. *B,* vIRF3 wt and tm2 mutant enhance HIF-1α protein expression in transient expression assay. 293T cells were transfected with HIF-1α expression vector (2 μg) along with increasing amounts (0, 1, or 2 μg) of vIRF1, vIRF3 wt, vIRF3 tm2, vIRF3 hm, or vIRF3 dd2. GST expression vector (0.5 μg) was included as a transfection control. Whole-cell lysates were analyzed by immunoblotting with anti-FLAG, anti-V5, and anti-GST antibodies to detect HIF-1α, vIRF, and GST expression. *C,* vIRF3 wt and vIRF3 tm2 mutant enhance HIF-1α transcriptional activity. 293T cells were transfected with HIF-1α expression vector, HRE-luciferase plasmid, and pRL-SV40 plasmid along with vIRF3 wt or its mutant expression vector. At 48 h after transfection, cells were harvested and firefly and *Renilla* luciferase values were measured. Firefly luciferase values were normalized to *Renilla* luciferase values for a transfection efficiency control and presented as a fold induction over vector-transfected cells.

additional expression of vIRF3 in these cells considerably enhanced HIF-1α level (Fig. 3*A*). Finally, 293T cells were transfected with the same amount of FLAG-HIF-1α (2 μg) expression vector along with increasing amounts (0, 1, and 2 μg) of V5-vIRF3 wt, tm2, hm, or dd2 mutant. V5-vIRF1 and GST expression vectors were included as negative controls. This showed that vIRF3 wt and vIRF3 tm2 that were capable of interacting with HIF-1α markedly increased HIF-1α protein expression. On the other hand, vIRF3 hm that weakly interacted with HIF-1α increased HIF-1α protein expression at a low level and vIRF3 dd2 that showed no interaction with HIF-1α did not affect HIF-1α protein expression (Fig. 3*B*). The effect of vIRF3 on HIF-1α expression was specific because vIRF3 did not affect GST expression nor did vIRF1 affect HIF-1α expression (Fig. 3*B*).

We subsequently tested whether the increase of HIF-1α expression induced by vIRF3 led to the increase of its transcriptional activity. 293T cells were transfected with HIF-1α expression vector and HRE-luciferase plasmid together with vIRF3 wt or its mutant expression vector. Consistent with their abilities to affect HIF-1α protein expression, vIRF3 wt detectably enhanced HIF-1α transcriptional activity, whereas vIRF3 hm and dd2 mutants were not able to do (Fig. 3*C*). These results indicate that vIRF3 wt

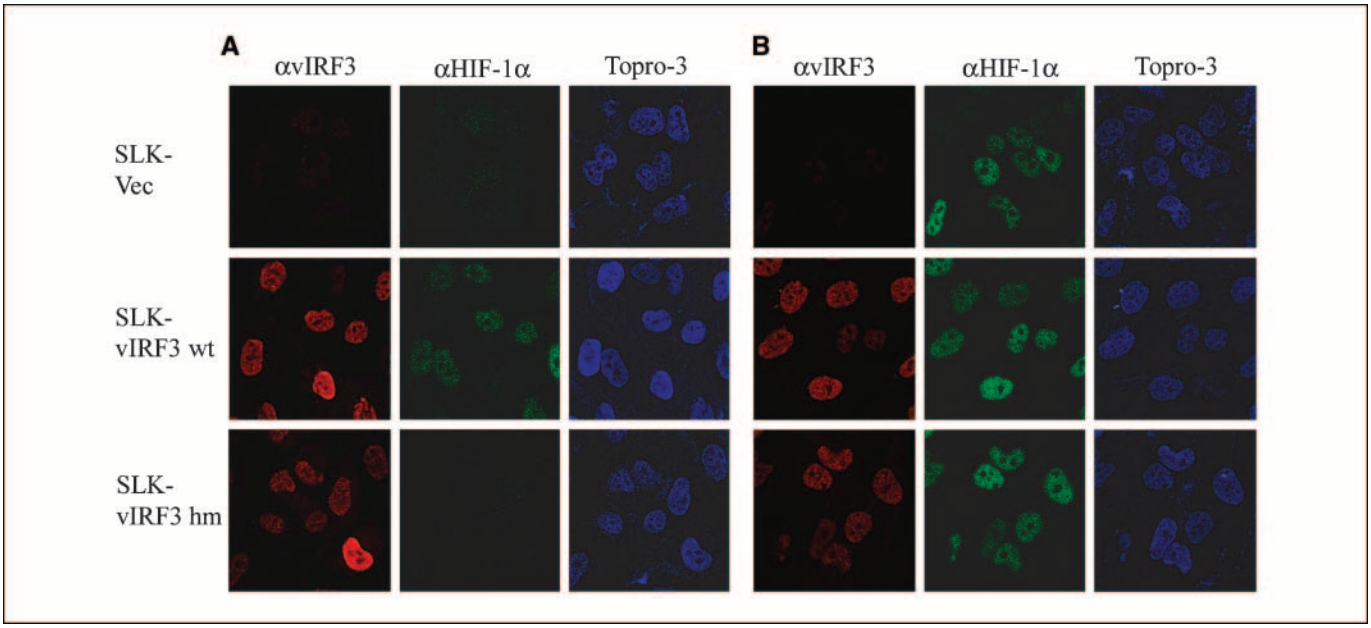

Figure 4. vIRF3 expression enhances HIF-1α nuclear localization. SLK-vector, SLK-vIRF3 wt, and SLK-vIRF3 hm cells were mock treated (*A*) or treated with 100 μmol/L cobalt chloride (*B*) for 12 h followed by confocal microscopy using anti-HIF-1α (*green*) and anti-vIRF3 (*red*) antibodies. Nucleus (*blue*) was detected with Topro-3 staining.

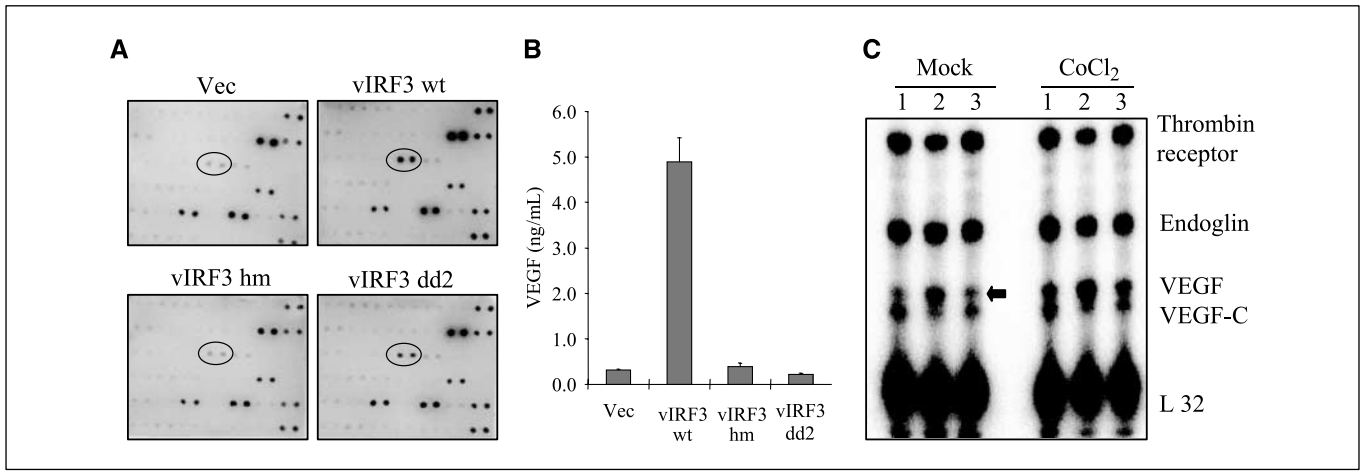

Figure 5. Induction of VEGF production by vIRF3. *A,* cytokine antibody array. The supernatants of SLK-vector, SLK-vIRF3 wt, SLK-vIRF3 hm, and SLK-vIRF3 dd2 cells were collected, spun down to remove cell debris, and subjected to cytokine antibody array. Antibody array was carried out according to the manufacturer's recommendation using cytokine array membranes (Panomics), which contained 36 cytokines/chemokines and 6 controls. Each cytokine was tested in duplicate and arranged as follows (from *left* to *right*): *1st row,* Apol/Fas, Leptin, Rantes, ICAM-1, IL-2, and IL-7 (positive control); *2nd row,* CTLA, MIP1α, TGFβ, VCAM-1, IL-3, and IL-8 (positive control); *3rd row,* Eotaxin, MIP1β, IFNγ, VEGF, IL-4, and IL-10 (negative control); *4th row,* GM-CSF, MIP4, TNFα, IL-1α, IL-5, and IL-12 (p40; negative control); *5th row,* EGF, MIP-5, TNFRI, IL-1β, IL-6, and IL-15 (positive control); *6th row,* IP-10, MMP3, TNFRII, IL-1Rα, IL-6R, and IL-17 (positive control). *Circles,* VEGF. *B,* VEGF ELISA. The supernatants from SLK cells were prepared as described in *A*. The concentration of VEGF was measured by ELISA according to the manufacturer's recommendation (BD PharMingen). Each test was done in duplicate. *Columns,* mean; *bars,* SE. *C,* RPA. SLK cells expressing vector (*lane 1*), vIRF3 wt (*lane 2*), or vIRF3 hm (*lane 3*) were mock treated or treated with cobalt chloride (*$CoCl_2$*) for 20 h. The total RNA (15 μg) isolated from each cell line was subjected to RPA using a RPA kit as described in Materials and Methods. *Arrow,* VEGF mRNA.

efficiently interacts with HIF-1α and strongly activates its transcriptional activity. In contrast, vIRF3 hm and vIRF3 dd2 mutants do not interact with HIF-1α nor activate its transcriptional activity. Despite its efficient interaction with HIF-1α, however, vIRF3 tm2 mutant activated HIF-1α transcriptional activity at the reduced level compared with vIRF3 wt (Fig. 3*C*). Thus, although HIF-1α stabilization is dependent primarily on its interaction with vIRF3, additional factor(s) other than interaction may be necessary for vIRF3 to efficiently activate HIF-1α transcription factor activity.

vIRF3 induces HIF-1α nuclear accumulation. Under normoxic conditions, HIF-1α is ubiquitinated and rapidly degraded by the proteasome, resulting in its short half-life (90 seconds), and because of which, the detection of HIF-1α is extremely difficult (36). Under hypoxic conditions, however, HIF-1α is stabilized, accumulated, and translocalized into the nucleus where it forms a heterodimeric complex with HIF-1β to activate its target gene transcriptions (37). Confocal microscopy showed that the HIF-1α protein was readily detected in the nucleus of SLK-vIRF3 cells, whereas it was not detectable in SLK-vector cells and SLK-vIRF3 hm cells (Fig. 4*A*). On the other hand, on cobalt chloride treatment, which mimics hypoxic conditions, HIF-1α was readily detected in the nucleus of all three cell lines at equivalent levels (Fig. 4*B*). It should be noteworthy that a few cells expressing vIRF3 wt did not show the visible nuclear accumulation of HIF-1α and vice versa. Nevertheless, the majority of vIRF3-expressing cells showed considerable nuclear accumulation of HIF-1α. This indicates that vIRF3 expression apparently results in HIF-1α nuclear accumulation.

vIRF3 promotes VEGF production. It has been proposed that cytokines, chemokines, and angiogenic factors play key roles in the development of Kaposi's sarcoma pathogenesis (4). Because vIRF3 robustly increased HIF-1α amount, we tested the effect of vIRF3 expression on cellular cytokine production using a cytokine antibody array. This procedure uses a sandwich immunoblot assay to profile the expression of cellular cytokines and chemokines. It showed that vIRF3 wt expression significantly induced VEGF production without affecting the production of other cytokine (Fig. 5*A*). In contrast, vIRF3 hm and dd2 mutant expression showed minimal effects on VEGF or other cytokine production under the same conditions (Fig. 5*A*). ELISA was then performed to quantify VEGF produced from SLK cells expressing vector, vIRF3 wt, hm, or dd2 mutant. Consistent with its ability to induce HIF-1α stabilization and transcriptional activity, vIRF3 wt expression significantly induced VEGF production (Fig. 5*B*).

To further confirm vIRF3-mediated cytokine production, we performed RPA. The total mRNAs were prepared from the SLK stable cells and hybridized with *in vitro*–transcribed probes, which contained cRNA to VEGF, as well as several other signal transducers related to angiogenesis. VEGF mRNA level was markedly induced in SLK-vIRF3 wt cells when compared with SLK-vector and SLK-vIRF3 hm cells (Fig. 5*C*). Although overall VEGF mRNA level was elevated by cobalt chloride treatment, it was still higher in SLK-vIRF3 wt cells than in SLK-vector or SLK-vIRF3 hm cells (Fig. 5*C*). Despite the slight increase of VEGF amount in vIRF3 dd2 mutant-expressing cells from cytokine array, it should be noted that this increase was not detected in ELISA and RPA analysis (Fig. 5). These results indicate that the vIRF3-mediated stabilization of HIF-1α ultimately leads to the increase of VEGF expression.

vIRF3 promotes endothelial tube formation. Kaposi's sarcoma has been characterized as a hypervascular tumor accompanied by highly induced VEGF around its lesion (4). To assess the biological role of enhanced VEGF production, human umbilical vein endothelial cells (HUVECs) were used for tube formation assay. In principle, cells on ECM gel from Engelbreth-Holm-Swarm murine sarcoma respond to angiogenic growth factors and migrate to form hexagonal tubes. The conditioned media from SLK-vector, SLK-vIRF3 wt, SLK-vIRF3 hm, or SLK-vIRF3 dd2 cell cultures were evaluated for their ability to induce tube formation of HUVECs

(Fig. 6). As a positive control, VEGF cytokine was added (*panel 2*) into the endothelial basal medium. Active tube formation was observed in HUVECs with the conditioned medium of SLK-vIRF3 wt cells (*panel 4*) but was negligible with the conditioned medium of SLK-vector, SLK-vIRF3 hm, or SLK-vIRF3 dd2 cells (*panels 3, 5*, and *6*). The addition of VEGF neutralizing antibody effectively inhibited the endothelial tube formations induced by VEGF (*panel 7*) and the conditioned medium of SLK-vIRF3 wt cells (*panel 8*). This result shows that vIRF3 induces VEGF cytokine production, leading to the active endothelial tube formation.

Discussion

Signal transduction under hypoxic conditions is essential for tumor cell growth, supplying the metabolical needs of outgrowing tumor cells (38). HIF-1α is the master regulator in hypoxic signal transduction, and therefore, its regulation is directly influenced by the oxygen concentration around the cells. Viral proteins often exploit this pathway to facilitate virus-induced oncogenesis. It has been shown that KSHV vGPCR activates, through the phosphorylation of HIF-1α protein, the promoter activity driven by HRE sequence isolated from VEGF promoter region (10). Surprisingly, we did not observe the detectable increase of HRE-driven promoter activity on vGPCR expression. The HRE sequences used by the previous study (TACGTGGG; ref. 10) and by us (GGATACGTGACC) are similar to each other by sharing the core "TACGTC" sequence but different at their 5′ and 3′ regions of the core nucleotide sequence. Because the HRE-driven promoter sequences in both studies are short, the regions flanking the core sequence might be critical for the specificity. Furthermore, whereas the previous report (10) used expression of both HIF-1α and HIF-1β to show the vGPCR-induced activation of HRE promoter activity, we used HIF-1α expression only to show vIRF3-induced HRE promoter activity. The different outcomes between the previous report (10) and ours may be due to the different experimental conditions.

The latent infection of KSHV in primary human dermal microvascular endothelial cells and human telomerase-immortalized microvascular endothelial cells increases the HIF-1α and HIF-2α protein levels, although the viral protein causing this deregulation has not yet been identified (33). Besides the deregulation of HIF-1α, KSHV has developed various ways to respond to hypoxia, resulting in the induction of viral lytic replication (39). In fact, HRE sequences are present in the promoter regions of RTA and ORF34 of KSHV genome (40). This indicates that hypoxia signal transduction and its deregulation by viral proteins are important aspects of KSHV life cycle and potentially pathogenesis.

One of the major transcriptional targets of HIF-1α is VEGF, which is a potent angiogenic stimulator. The high level of VEGF expression seen in Kaposi's sarcoma lesions may correlate with the fact that KSHV encodes several viral proteins that deregulate HIF-1α/VEGF pathway (10, 11, 41). Here, we show that vIRF3 induces VEGF production in SLK endothelial cells by stabilizing HIF-1α protein. However, the expression of vIRF3 has not been detected in Kaposi's sarcoma lesions (25). Only a few KSHV genes (*LANA1, vFLIP, vCyclin*, and *Kaposin*) have been detectably expressed in the late stage of Kaposi's sarcoma lesions, suggesting that they have critical role(s) in the progression and maintenance of Kaposi's sarcoma lesions (42). However, neither *vCyclin* nor *vFLIP* nor *Kaposin* displays detectable angiogenic tumor activity in mice (12), although they have strong oncogenic potentials *in vitro* (43, 44). Therefore, the great enigma of KSHV pathogenesis is why many KSHV genes with some form of *in vitro* transforming or potentially transforming properties fall into lytic cycle genes rather than into latent genes (45). Although the lytic cycle in herpesviruses is normally a process that leads to cell death, the pattern of lytic cycle expression in PELs, MCDs, and Kaposi's sarcoma lesions suggests an abortive lytic cycle where some cells express only a few lytic genes (45). Thus, it has been speculated that some forms of abortive lytic replication may promote viral pathogenesis without the death of host cells (45). The most well-characterized KSHV lytic gene in this matter is *vGPCR*. It is expressed in the early lytic cycle in both PELs and virus-infected endothelial cells but is not expressed at detectable levels in the vast majority of latently infected cells. Another examples are the KSHV *K3* and *K5* genes: endothelial cells latently infected with KSHV show drastic reduction of surface expression of MHC class I, ICAM-1, and PECAM, which is primarily mediated by K3 and K5 lytic proteins. It suggests that lytic genes are intermittently expressed in latently infected cells and contribute to the virus-induced phenotype without the complete cycle of lytic replication and cell death (46). Here, we have shown that vIRF3 robustly induces HIF-1α protein stability and thereby VEGF production, which may affect the proliferation of neighboring cells by a paracrine mechanism. Thus, it is likely that KSHV has evolved an unconventional strategy by using lytic cycle proteins to deregulate cellular proliferation control, which ultimately contributes to virus-associated pathogenesis.

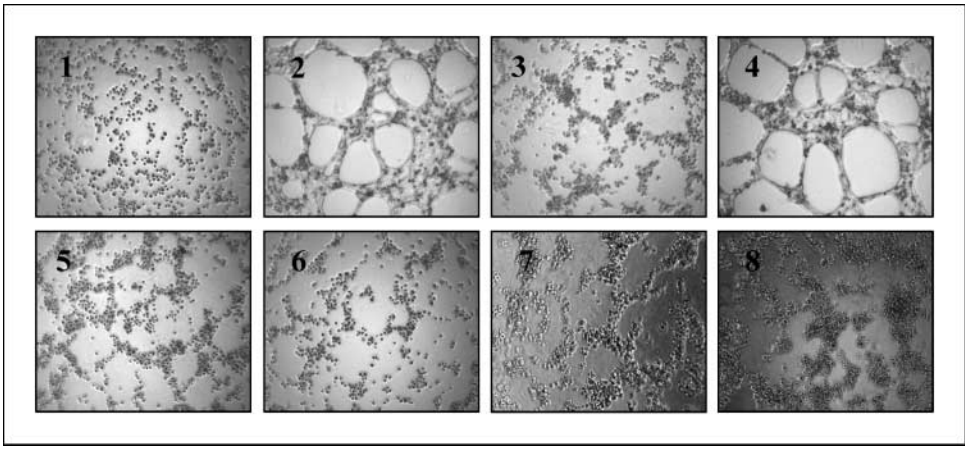

Figure 6. vIRF3 expression facilitates endothelial tube formation. The conditioned medium from SLK cells expressing vector (*panel 3*), vIRF3 wt (*panels 4* and *8*), vIRF3 hm (*panel 5*), or vIRF3 dd2 (*panel 6*) was tested for tube formation assay. For the controls, DMEM (*panel 1*) or DMEM supplemented with VEGF (*panels 2* and *7*) was added. In panels 7 and 8, the VEGF neutralizing antibody was added.

One of the questions that need to be addressed is how vIRF3 stabilizes HIF-1α protein. In a recent study by Mylonis et al. (47), the phosphorylation of HIF-1α facilitates its nuclear retention, which results in HIF-1α stabilization; otherwise, it undergoes ubiquitination and degradation in the cytoplasm. Consistent with this, HIF-1α was primarily accumulated in the nucleus in vIRF3 wt-expressing cells (Fig. 4*A*). However, the cellular compartment where HIF-1α is ubiquitinated and degraded is not completely understood (48). It has been speculated that HIF-1α is ubiquitinated and degraded in the cytoplasm and that only the stabilized HIF-1α moves into the nucleus for its transcriptional activation of target genes. On the other hand, an alternate mechanism has been proposed: a newly synthesized HIF-1α is immediately imported into the nucleus for ubiquitination and subsequently exported into the cytoplasm for degradation (36). Regardless of the cellular regulatory mechanisms of HIF-1α degradation, however, it is reasonable to speculate that the KSHV vIRF3 recruits HIF-1α into the nucleus, which consequently keeps HIF-1α from degradation.

The ubiquitination of HIF-1α by the VHL complex is the most critical factor for HIF-1α degradation (20). We initially hypothesized that vIRF3 stabilized HIF-1α protein by either disrupting VHL complex formation and/or inhibiting its E3 ubiquitin ligase activity. However, we found that vIRF3 affected neither VHL complex formation nor VHL complex activity at any detectable levels.[3] This indicates that vIRF3 uses a novel strategy to up-regulate HIF-1α protein stability. Additional studies are needed to elucidate the specific mechanism by which vIRF3 stabilizes HIF-1α.

In summary, we have shown that KSHV vIRF3 specifically interacts with HIF-1α subunit and this interaction leads to HIF-1α protein stabilization and transcriptional activation, which in turn induces VEGF expression and ultimately facilitates endothelial tube formation. This indicates that KSHV has evolved to acquire a viral homologue of the cellular *IRF* gene to enhance HIF-1α protein stability and transcriptional activity, which may contribute to viral pathogenesis.

[3] Unpublished results.

Acknowledgments

Received 7/19/2007; revised 12/4/2007; accepted 1/11/2008.

Grant support: USPHS grants CA106156, CA82057, CA91819, CA115284, and RR00168 (J.U. Jung), exchange program between Harvard Medical School and the graduate training program 1071 at the Friedrich-Alexander University Erlangen-Nuremberg, Germany (M.U. Gack), and Korea Research Foundation grant KRF-2005-214-C00104 (C-H. Joo).

The costs of publication of this article were defrayed in part by the payment of page charges. This article must therefore be hereby marked *advertisement* in accordance with 18 U.S.C. Section 1734 solely to indicate this fact.

We thank Drs. Patrick S. Moore and Chris Bradfield for providing the plasmids encoding vIRF3 and HIF-1α, respectively.

References

1. Dupin N, Grandadam M, Calvez V, et al. Herpesvirus-like DNA sequences in patients with Mediterranean Kaposi's sarcoma. Lancet 1995;345:761–2.
2. Cesarman E, Chang Y, Moore PS, Said JW, Knowles DM. Kaposi's sarcoma-associated herpesvirus-like DNA sequences in AIDS-related body-cavity-based lymphomas. N Engl J Med 1995;332:1186–91.
3. Soulier J, Grollet L, Oksenhendler E, et al. Kaposi's sarcoma-associated herpesvirus-like DNA sequences in multicentric Castleman's disease. Blood 1995;86:1276–80.
4. Cornali E, Zietz C, Benelli R, et al. Vascular endothelial growth factor regulates angiogenesis and vascular permeability in Kaposi's sarcoma. Am J Pathol 1996;149:1851–69.
5. Longo DL, Steis RG, Lane HC, et al. Malignancies in the AIDS patient: natural history, treatment strategies, and preliminary results. Ann N Y Acad Sci 1984;437:421–30.
6. Kaaya EE, Parravicini C, Ordonez C, et al. Heterogeneity of spindle cells in Kaposi's sarcoma: comparison of cells in lesions and in culture. J Acquir Immune Defic Syndr Hum Retrovirol 1995;10:295–305.
7. Boshoff C, Schulz TF, Kennedy MM, et al. Kaposi's sarcoma-associated herpesvirus infects endothelial and spindle cells. Nat Med 1995;1:1274–8.
8. Ganem D. KSHV and Kaposi's sarcoma: the end of the beginning? Cell 1997;91:157–60.
9. Arvanitakis L, Geras-Raaka E, Varma A, Gershengorn MC, Cesarman E. Human herpesvirus KSHV encodes a constitutively active G-protein-coupled receptor linked to cell proliferation. Nature 1997;385:347–50.
10. Sodhi A, Montaner S, Patel V, et al. The Kaposi's sarcoma-associated herpes virus G protein-coupled receptor up-regulates vascular endothelial growth factor expression and secretion through mitogen-activated protein kinase and p38 pathways acting on hypoxia-inducible factor 1α. Cancer Res 2000;60:4873–80.
11. Bais C, Santomasso B, Coso O, et al. G-protein-coupled receptor of Kaposi's sarcoma-associated herpesvirus is a viral oncogene and angiogenesis activator. Nature 1998;391:86–9.
12. Montaner S, Sodhi A, Molinolo A, et al. Endothelial infection with KSHV genes *in vivo* reveals that vGPCR initiates Kaposi's sarcomagenesis and can promote the tumorigenic potential of viral latent genes. Cancer Cell 2003;3:23–36.
13. Cesarman E, Mesri EA, Gershengorn MC. Viral G protein-coupled receptor and Kaposi's sarcoma: a model of paracrine neoplasia? J Exp Med 2000;191:417–22.
14. Wang L, Wakisaka N, Tomlinson CC, et al. The Kaposi's sarcoma-associated herpesvirus (KSHV/HHV-8) K1 protein induces expression of angiogenic and invasion factors. Cancer Res 2004;64:2774–81.
15. Aoki Y, Jaffe ES, Chang Y, et al. Angiogenesis and hematopoiesis induced by Kaposi's sarcoma-associated herpesvirus-encoded interleukin-6. Blood 1999;93:4034–43.
16. Masood R, Cai J, Zheng T, Smith DL, Naidu Y, Gill PS. Vascular endothelial growth factor/vascular permeability factor is an autocrine growth factor for AIDS-Kaposi sarcoma. Proc Natl Acad Sci U S A 1997;94:979–84.
17. Wang GL, Jiang BH, Rue EA, Semenza GL. Hypoxia-inducible factor 1 is a basic-helix-loop-helix-PAS heterodimer regulated by cellular O_2 tension. Proc Natl Acad Sci U S A 1995;92:5510–4.
18. Kamura T, Sato S, Iwai K, Czyzyk-Krzeska M, Conaway RC, Conaway JW. Activation of HIF1α ubiquitination by a reconstituted von Hippel-Lindau (VHL) tumor suppressor complex. Proc Natl Acad Sci U S A 2000;97:10430–5.
19. Ivan M, Kondo K, Yang H, et al. HIFα targeted for VHL-mediated destruction by proline hydroxylation: implications for O_2 sensing. Science 2001;292:464–8.
20. Tanimoto K, Makino Y, Pereira T, Poellinger L. Mechanism of regulation of the hypoxia-inducible factor-1α by the von Hippel-Lindau tumor suppressor protein. EMBO J 2000;19:4298–309.
21. Forsythe JA, Jiang BH, Iyer NV, et al. Activation of vascular endothelial growth factor gene transcription by hypoxia-inducible factor 1. Mol Cell Biol 1996;16:4604–13.
22. Semenza GL, Wang GL. A nuclear factor induced by hypoxia via *de novo* protein synthesis binds to the human erythropoietin gene enhancer at a site required for transcriptional activation. Mol Cell Biol 1992;12:5447–54.
23. Semenza GL, Roth PH, Fang HM, Wang GL. Transcriptional regulation of genes encoding glycolytic enzymes by hypoxia-inducible factor 1. J Biol Chem 1994;269:23757–63.
24. Gnarra JR, Tory K, Weng Y, et al. Mutations of the VHL tumour suppressor gene in renal carcinoma. Nat Genet 1994;7:85–90.
25. Rivas C, Thlick AE, Parravicini C, Moore PS, Chang Y. Kaposi's sarcoma-associated herpesvirus LANA2 is a B-cell-specific latent viral protein that inhibits p53. J Virol 2001;75:429–38.
26. Lubyova B, Pitha PM. Characterization of a novel human herpesvirus 8-encoded protein, vIRF-3, that shows homology to viral and cellular interferon regulatory factors. J Virol 2000;74:8194–201.
27. Esteban M, Garcia MA, Domingo-Gil E, Arroyo J, Nombela C, Rivas C. The latency protein LANA2 from Kaposi's sarcoma-associated herpesvirus inhibits apoptosis induced by dsRNA-activated protein kinase but not RNase L activation. J Gen Virol 2003;84:1463–70.
28. Lubyova B, Kellum MJ, Frisancho AJ, Pitha PM. Kaposi's sarcoma-associated herpesvirus-encoded vIRF-3 stimulates the transcriptional activity of cellular IRF-3 and IRF-7. J Biol Chem 2004;279:7643–54.
29. Joo CH, Shin YC, Gack M, Wu L, Levy D, Jung JU. Inhibition of IRF7-mediated interferon signal transduction by Kaposi's sarcoma-associated herpesvirus vIRF3. J Virol 2007;81:8282–92.
30. Hobbs S, Jitrapakdee S, Wallace JC. Development of a bicistronic vector driven by the human polypeptide chain elongation factor 1α promoter for creation of stable mammalian cell lines that express very high levels of recombinant proteins. Biochem Biophys Res Commun 1998;252:368–72.
31. Pfaffl MW. A new mathematical model for relative quantification in real-time RT-PCR. Nucleic Acids Res 2001;29:e45.
32. Nakamura H, Li M, Zarycki J, Jung JU. Inhibition of p53 tumor suppressor by viral interferon regulatory factor. J Virol 2001;75:7572–82.
33. Carroll PA, Kenerson HL, Yeung RS, Lagunoff M. Latent Kaposi's sarcoma-associated herpesvirus infection of endothelial cells activates hypoxia-induced factors. J Virol 2006;80:10802–12.
34. Kaelin WG. Proline hydroxylation and gene expression. Annu Rev Biochem 2005;74:115–28.
35. Yuan Y, Hilliard G, Ferguson T, Millhorn DE. Cobalt inhibits the interaction between hypoxia-inducible

factor-α and von Hippel-Lindau protein by direct binding to hypoxia-inducible factor-α. J Biol Chem 2003;278:15911–6.
36. Groulx I, Lee S. Oxygen-dependent ubiquitination and degradation of hypoxia-inducible factor requires nuclear-cytoplasmic trafficking of the von Hippel-Lindau tumor suppressor protein. Mol Cell Biol 2002; 22:5319–36.
37. Kallio PJ, Okamoto K, O'Brien S, et al. Signal transduction in hypoxic cells: inducible nuclear translocation and recruitment of the CBP/p300 coactivator by the hypoxia-inducible factor-1α. EMBO J 1998;17: 6573–86.
38. Brahimi-Horn C, Berra E, Pouyssegur J. Hypoxia: the tumor's gateway to progression along the angiogenic pathway. Trends Cell Biol 2001;11:S32–6.
39. Davis DA, Rinderknecht AS, Zoeteweij JP, et al. Hypoxia induces lytic replication of Kaposi sarcoma-associated herpesvirus. Blood 2001;97:3244–50.
40. Haque M, Davis DA, Wang V, Widmer I, Yarchoan R. Kaposi's sarcoma-associated herpesvirus (human herpesvirus 8) contains hypoxia response elements: relevance to lytic induction by hypoxia. J Virol 2003;77: 6761–8.
41. Cai Q, Lan K, Verma SC, Si H, Lin D, Robertson ES. Kaposi's sarcoma-associated herpesvirus latent protein LANA interacts with HIF-1α to upregulate RTA expression during hypoxia: latency control under low oxygen conditions. J Virol 2006;80: 7965–75.
42. Jenner RG, Boshoff C. The molecular pathology of Kaposi's sarcoma-associated herpesvirus. Biochim Biophys Acta 2002;1602:1–22.
43. Djerbi M, Screpanti V, Catrina AI, Bogen B, Biberfeld P, Grandien A. The inhibitor of death receptor signaling, FLICE-inhibitory protein defines a new class of tumor progression factors. J Exp Med 1999;190:1025–32.
44. Muralidhar S, Pumfery AM, Hassani M, et al. Identification of kaposin (open reading frame K12) as a human herpesvirus 8 (Kaposi's sarcoma-associated herpesvirus) transforming gene. J Virol 1998;72:4980–8.
45. Hayward GS. Initiation of angiogenic Kaposi's sarcoma lesions. Cancer Cell 2003;3:1–3.
46. Tomescu C, Law WK, Kedes DH. Surface down-regulation of major histocompatibility complex class I, PE-CAM, and ICAM-1 following *de novo* infection of endothelial cells with Kaposi's sarcoma-associated herpesvirus. J Virol 2003;77:9669–84.
47. Mylonis I, Chachami G, Samiotaki M, et al. Identification of MAPK phosphorylation sites and their role in the localization and activity of hypoxia-inducible factor-1α. J Biol Chem 2006;281:33095–106.
48. Zheng X, Ruas JL, Cao R, et al. Cell-type-specific regulation of degradation of hypoxia-inducible factor 1α: role of subcellular compartmentalization. Mol Cell Biol 2006;26:4628–41.